Journal of Radioanalytical and Nuclear Chemistry (2023) 332:3719–3732
https://doi.org/10.1007/s10967-023-09064-3

Sorption behavior of Sr(II) in granitic rock: the effect of MX-80 bentonite colloids

Noora Pakkanen[1] · Eini Puhakka[1] · Marja Siitari-Kauppi[1] · Pirkko Hölttä[1]

Received: 24 March 2023 / Accepted: 19 July 2023 / Published online: 8 August 2023

Abstract
MX-80 bentonite colloids' effect on radionuclide sorption was studied by batch method and transport in flow using a granitic drill core column and Sr(II) as a radionuclide. Batch-type sorption and desorption experiments were conducted to determine Sr(II)'s distribution coefficients on bentonite colloids and metatexitic gneiss. Molecular modeling assessed the radionuclide's sorption affinity and justified the differences in Sr(II)'s sorption behavior on biotite versus montmorillonite. The distribution coefficients were found to be a hundred times greater for colloids than for granitic rock. Strontium's breakthrough from the column with bentonite colloids was successful without notable retardation on rock minerals.

Keywords Sorption · Strontium(II) · Montmorillonite · Colloids · Granitic rock · Flow

Introduction

Strontium isotope ^{90}Sr is one of the most crucial and hazardous products of uranium and plutonium fission as well as one of the main radionuclide wastes generated in nuclear fuel processing. ^{90}Sr, alongside ^{137}Cs, is responsible for most of the radioactivity in nuclear waste during the first few 100 years. In Finland and Sweden, the final disposal of spent nuclear fuel (SNF) i.e., high-level nuclear waste is considered to take place in deep geological repositories such as the Onkalo spent nuclear fuel repository built below the surface of Olkiluoto island in Western Finland. According to the KBS-3 multiple barrier concept, these repositories are surrounded by bedrock in stable granitic-type rock formations [1–4]. The repository system has been designed to isolate harmful radionuclides and prevent their migration into the groundwater system during containment failure [5]. By utilizing multiple engineered and natural barriers, failure of one barrier will not endanger radionuclide isolation [6].

Many decades of work have been performed to understand the functionality of the Engineered Barrier System (EBS) [7–9]. One engineered barrier material is bentonite clay, which has formed out of volcanic ash and has a very high montmorillonite (swelling smectite clay) content [10, 11]. Raw and unpurified natural bentonites may also include accessory minerals such as quartz, feldspar, and pyrite [11, 12]. The amount of organic matter and oxides varies between bentonites with different geochemical backgrounds and formation environments. Composition affects bentonite's colloidal properties, such as the colloid's surface chemistry and its tendency to aggregate [10, 11, 13]. In general, clay minerals based on bentonite may exhibit the properties of thixotropic-gel formation with water, high water absorption, and high cation-exchange capacity [14]. These properties can vary in clay minerals depending upon the nature of interstitial water, and exchangeable cations in the interlayer space.

Bentonite was proposed to be used as a buffer material in SNF repositories due to its suitable characteristics such as high sorption capacity and plasticity, good swelling properties, high pH buffering capacity, and low hydraulic conductivity. Once bentonite comes in contact with water it starts to swell and block transport pathways of the bedrock adjacent to the bentonite barrier including microfractures and pores. With these characteristics, bentonite buffer could provide the needed mechanical protection for the SNF canister, while maintaining a stable chemical environment [11, 15].

Even with a multiple barrier system, it is possible that several barriers fail, and radionuclide isolation will be compromised. In case of canister failure, SNF radionuclides can start migrating outside of the repository area and into the surrounding bedrock and groundwater system.

✉ Noora Pakkanen
noora.m.pakkanen@helsinki.fi

[1] Department of Chemistry, University of Helsinki, P.O. Box 55, 00014 Helsinki, Finland

Once leaked, the SNF radionuclides can pose a serious threat to humans and animals alike. As reported previously in the literature, the radionuclide retardation from flowing water in rock fractures is mainly based on diffusional transport into the rock's connected pores and sorption on solid mineral surfaces [16, 17]. Several in situ and laboratory experiments have proven that matrix diffusion of radioactive elements exists and that the retardation of—for example, cesium, strontium, and barium—is strongly dependent on their high sorption on rock's main minerals [18, 19]. For example, biotite, which is one of the main minerals in Olkiluoto island's main rock type metatexitic gneiss, has been observed to sorb radionuclides effectively [20–22].

The use of colloidal bentonite clay has been considered in the long–term safety assessment of an SNF repository even though colloid-facilitated transport of radionuclides may significantly contribute to the repository's long-term performance. Several studies have indicated radionuclide (especially actinide) sorption on colloids and the mobility of radiocolloids in fracture flow. For example, field-scale studies at hazardous waste sites have provided evidence that colloid transport can enhance actinide migration [23, 24] and laboratory experiments have confirmed that colloids can accelerate the transport of cationic and anionic metals through porous and fractured media [25, 26]. The potential relevance of colloids in radionuclide transport depends highly on several factors, such as colloid stability in different chemical environments, the mechanism of radionuclide interaction with colloids, and on the irreversibility of the radionuclide-colloid binding. Evidence shows, that despite of relevance of colloid transport being governed by prevailing environmental conditions, it is important that colloid transport of radionuclides is considered in the repository's safety assessment. For example, in Olkiluoto, the determined contents of natural inorganic and organic colloids in groundwater are currently low, but the bentonite buffer used in the EBS system can be seen as a potential source of colloids [27, 28]. Bentonite buffer's role as a colloid source is especially relevant in a post-glacial repository system, where bentonite buffer is seen as the greatest and most infinite source of colloids that can impact the repository's functionality greatly [29].

As radionuclides' sorption mechanisms are very complicated, molecular modeling can be used to interpret experimental findings and justify the sorption behavior of Sr(II) in rock minerals versus montmorillonite. In our earlier studies, molecular modeling has been utilized to study radionuclides' sorption on biotite's crystalline structure and its end-members phlogopite and annite. Especially, the focus has been on the phlogopite and its crystalline and surface structures (basal and edge sites) and sorption of Ni(II) [30], Ba(II) [21], Se(IV), and Se(VI) species [31].

Biotite $[K(Mg,Fe)_3AlSi_3O_{10}(OH,F)_2]$ with its end-members and montmorillonite $[Si_8(Al_{4-x}Mg_x)O_{20}(OH)_4M^{k+}{}_{x/k} \cdot nH_2O$, M = alkali/alkali earth metal cation, $x = 0.4 - 1.2]$ are phyllosilicates which are formed by superposed atomic planes parallel to the (001) face of the crystalline structure [10]. They have a prismatic and sheet-like structure, where cation layers connect the negatively charged layers. The negatively charged layers consist of tetrahedral (T) and octahedral (O) sheets that stack together to form 2:1 (TOT) layers with a characteristic repeat distance between them [32]. The negative framework charge is balanced by an equivalent number of cations on the internal and external basal planes and these ions are exchangeable to ions in external solutions. In biotite, these ions are non-hydrated, thus not readily exchangeable, while in montmorillonite hydrated and readily exchangeable.

The experimental work described here relates to an earlier experiment conducted in our laboratories by Voutilainen et al. [19] where the same metatexitic gneiss column was used with conservative tracers (HTO, ^{36}Cl). Thus, the boundary conditions of this work have been established. In this research work, the focus is aimed at how non-conservative and slightly sorbing tracer behaves in the same, well-defined experimental flow conditions. Besides using a non-conservative tracer, bentonite colloids were also introduced to the experimental system. Groundwater simulant with small ionic strength was used to imitate low saline groundwater conditions in a post-glacial repository system, where colloids are present.

The purpose of the study is to give a relation for strontium retardation from the flow between metatexitic gneiss and bentonite colloids in the artificial long fracture. Information about the transport and sorption behavior of Sr(II) was gathered to understand the meaning of bentonite colloids in the radionuclide migration process. The batch-type sorption and desorption experiments of Sr(II) on commercial bentonite colloids (MX-80) and crushed metatexitic gneiss were performed in two different pH conditions (pH 7 and pH 9) to understand better the sorption competition between MX-80 bentonite colloids and the minerals of metatexitic gneiss. The effect of MX-80 bentonite colloids on strontium transport in flow was investigated using a metatexitic gneiss drill core column, where Sr(II) was injected into a constant flow of diluted bentonite colloid solution. In parallel with the experimental work, molecular modeling was performed to assess the sorption affinity of Sr(II) on biotite and montmorillonite at the molecular level.

Theory

Distribution coefficient

Sorption was studied through the distribution coefficient K_d ($m^3\ kg^{-1}$) value, which describes the sorption's strength on

a substrate [33]. Radionuclide's mobility depends on its distribution between the mobile and stationary phases, and to determine the relation between these two phases, the distribution coefficient was calculated according to Eq. (1):

$$K_{\mathrm{d}} = \frac{A_0 - A_L}{m} \times \frac{V}{A_L} \tag{1}$$

where $A_0 - A_L$ is the activity in the solid phase (rock or colloid), V(ml) the volume of the solution, A_L is the activity of the supernatant and $m(g)$ is the weight of the crushed rock or colloid.

Sorption and desorption percentages were calculated according to Eq. (2):

$$\left(\frac{A_L}{A_0}\right) * 100\% \tag{2}$$

where A_0 is the initial activity in the solution.

Pseudo-second-order kinetic model

A pseudo-second-order kinetic model was used to describe contact time's effect on sorption uptake [34]. Equation (3) was used to fit the model on sorption data:

$$q_t = \frac{q_e^2 k_2 t}{1 + q_e k_2 t} \tag{3}$$

where q_t is the adsorbed capacity at time t ($m^3\ kg^{-1}$), q_e the equilibrium adsorption capacity ($m^3\ kg^{-1}$), k_2 is the rate constant and t is time.

Experimental

Materials

Granitic rock

Olkiluoto Island is located on the Southwest coast of Finland. According to the drill core analyses, the island's bedrock consists of metatexitic gneiss (43%), diatexitic gneiss (21%), granite pegmatoid (20%), non-migmatitic gneisses (9%), and tonalite-granodiorite-granite gneiss (8%) [35]. As metatexitic gneiss is the main rock type of Olkiluoto island, it was chosen to be used in the experiments.

Metatexitic gneiss is a subgroup of migmatitic gneiss, and it contains diversely elongated, folded, or stretched leucosomes with diameters from several millimeters up to 10 cm. Mineralogically heterogeneous metatexitic gneiss is mainly composed of biotite (29%), quartz (20%), potassium feldspar (10%), plagioclase (15%), and cordierite (7%). In addition, several accessory minerals such as muscovite, chlorite, sillimanite, epidote, garnet, and opaque minerals [36, 37] (Table 1) can also be found. Metatexitic gneiss's specific surface area has been determined to be 0.5–1.0 $m^2\ g^{-1} \pm 5\%$ with the BET method for crushed rock samples with grain sizes of 60.0–300.0 µm and 1.0–2.0 mm. The effective diffusion coefficient of $8.0 \times 10^{-14}\ m^2\ s^{-1}$ has been determined for bivalent ion Ba(II) in the metatexitic gneiss sample [21].

Rock material used in the sorption and column experiments was received from the REPRO site [38], which is located at the main characterization level (420 m below the surface) at ONKALO. The rock core was taken from the hole where the in situ WPDE experiments [39] in ONKALO were performed [37, 40]. Before being used in this experiment, the column experiment´s structurally very heterogeneous metatexitic gneiss rock core had been used previously by Voutilainen et al. [19] in flow experiments with conservative tracers.

Table 1 Composition of materials [36, 37, 41]

Material	Porosity	Minerals	Composition (w%)
Metatexitic gneiss	0.5–1.0%	Biotite	28.5
		Quartz	28.1
		Potassium feldspar	15.0
		Plagioclase	14.2
		Cordierite	6.6
		Sillimanite	4.5
		Muscovite	2.0
		Chlorite	0.8
		Garnet	0.2
		Opaque	0.2
		Epidote	0.1
MX-80		Smectite	79.1
		Muscovite	7.5
		Quartz	4.4
		Calcite	3.1
		Tridymite	1.9
		Plagioclase	1.7
		Gypsum	1.3
		Magnetite	1.1
		Illite	0.6
		Pyrite	0.6
		Cristobalite	0.5
		Anatase	0.2
		Hematite	0.1
		Zircon	0.1

MX-80 bentonite

The source of colloids in this experiment was commercial non-purified and sodium-rich Wyoming Volclay MX-80 bentonite, which has been characterized previously by Kumpulainen and Kiviranta [41] and Vuorinen and Snellman [42]. The ratio of chemical components in MX-80 may vary due to its chemically inhomogeneous nature, but the typical composition is presented in Table 1. The main mineral group of MX-80 is smectites, which are crystalline, 2:1 layered hydrated aluminosilicates, that can swell when in contact with water and their structural cations can be exchanged. The stoichiometric formula of MX-80 can be described with the formula $(Si_{7.65}Al_{0.35})$ $(Al_{3.09}Fe(III)_{0.38}Mg_{0.56})$ $Na_{0.54}Ca_{0.08}Mg_{0.06}O_{20}(OH)_4$ [41]. The specific surface area of montmorillonite (smectite clay) particles has been determined to vary between 760 and 810 $m^2\ g^{-1}$ for particle sizes 100–1000 nm [43].

Synthetic granitic groundwater

Used low-salinity groundwater was so-called "Allard water" ($I = 0.005$ M) which is the median water from low-salinity groundwaters in Sweden [44]. For the preparation of Allard water [42, 44], MilliQ water and six basic solutions were used (Table 2).

Colloid solution

The colloid solution was prepared by mixing 400 mL of Allard water with 10 g of MX-80 bentonite powder. After mixing, the solution was placed into a shaker for a minimum of two weeks. Once ready, the colloid solution was centrifuged at a speed of 4000 rpm for 40 min. The liquid phase was carefully separated from the clay material and followed by particle size and concentration measurements. Solutions with particle sizes less than 500 nm were used for the final colloid solution. Colloids were characterized with scanning electron microscopy and Malvern's Zetasizer Nano ZS was used to determine the size of colloid-like particles as well as the colloid concentration of the created solution.

Table 2 Composition of Allard water [44] in pH 7

Chemical compound	M (mmol/L)
KCl	0.10
$CaCl_2 \cdot 2H_2O$	0.45
$Na_2SiO_3 \cdot 9H_2O$	0.12
$NaHCO_3$	2.01
$MgSO_4 \cdot 7H_2O$	0.1
$MgCl_2 \cdot 6H_2O$	0.08

Strontium

The strontium isotope ^{85}Sr was used in the experiments. In ^{235}U fission products, strontium appears in tracer amounts [45]. It has a half-life of 64.84 days, and it decays mainly by electronic capture into ^{85}Rb. ^{85}Sr has a gamma energy of 0.514 MeV with an intensity of 96%. In nature, strontium appears in oxidation state Sr(II) and its main adsorption mechanism is cation exchange. At higher pHs, ionic strengths, and in the presence of carbonate, adsorption through surface complexation increases [46, 47]. Strontium is known to have moderate sorption capacity due to its small size and large hydration sphere. It shares these chemical properties with other bivalent Ca(II) and Ba(II) ions.

The ^{85}Sr stock solution used in the experiments had a specific activity of 641.95 MBq mg^{-1} (Ref. Date 26.6.2018) and it was produced by Perkin Elmer. The activity of 0.58 kBq g^{-1} ($= 10^{-12}$ M) was used in the batch sorption experiments and 10.18 kBq was injected as a pulse through a 0.5 mL injection loop in the column experiment.

Methods

Batch sorption/desorption

Batch sorption experiments were commenced by grinding the metatexitic gneiss rock material into 1.25–2.00 mm-sized rubble. Crushed metatexitic gneiss was washed and equilibrated for nine days with Allard water. During the equilibration phase, water was changed to fresh Allard water on the third and sixth days of equilibration.

After equilibration, crushed metatexitic gneiss was combined with 9 mL of colloid solution, which had been equilibrated with 5 kBq of ^{85}Sr tracer solution for one day. The pH of a solution was set to values 7 or 9 and then placed within a shaker. Samples were left in the shaker for four different preselected times: 1 day, 4 days, 1 week, and 3 weeks. Two parallel samples were used for each experimental scenario.

Once the preselected time had passed, samples were centrifuged for 30 min with a speed of 2700 rpm to end the experiment and to separate the colloid solution and crushed metatexitic gneiss from each other. 1 mL of separated sample solution was gathered for immediate activity measurements to determine the activity sorbed on the crushed rock, and 4 mL of solution was transferred to ultracentrifuge tubes to determine the portion of Sr(II) sorbed on colloid surfaces. 4 mL samples were ultracentrifuged for 40 min with the speed of 90,000 rpm to separate colloid-like particles from the solution.

After ultracentrifugation, sample solutions were carefully pipetted from ultracentrifuge tubes, weighed, and put to activity measurement in Hidex Automatic Gamma Counter

(AGC) to determine activity retained on colloids. Finally, the equilibrium pH of the samples was measured.

Next desorption experiments were performed. Fresh Allard water was added to the sample tubes with crushed metatexitic gneiss that had been used before in the sorption experiments, and their pH was set. Samples were placed in a shaker and left there for 1 day, 4 days, 1 week, and 3 weeks. The experiment was finished by centrifuging the samples with ultracentrifuge and with the same settings as used previously in the batch sorption experiments. After ultracentrifugation, the solution was extracted from ultracentrifuge tubes and weighed, followed by activity, particle size, equilibrium pH, and concentration measurements.

Column experiment

The column experiment was conducted with a metatexitic gneiss drill core column that had a 0.1030 m^3 large surface area [19, 37]. The intact drill core, 80 cm in height and 42 mm in width was placed in an acrylic tube with a diameter of 46 mm and height of 80 cm, forming a flow channel of about 2 mm wide between the rock and the tube. Besides the flow channel, the experimental setup consisted of a peristaltic pump, radionuclide injection system, and fraction collector with a sample volume of 5 mL. The column had a total colloid solution volume of 221 mL and the experiments were performed under ambient air conditions. The colloid solution was pumped continuously through the column and the tracer was injected as a pulse through an injection loop with a known volume. The solution flowing from the column was fed to a fraction collector. A flow rate of 50 µL min^{-1} was generated and controlled with a peristaltic pump. Colloid solution with particle sizes of 300–500 nm and derived count rate varying between 900 and 1200 kcps was fed to the column throughout the whole experiment. ^{85}Sr activities of collected samples were measured and determined as a function of time. The column's flow field had already been characterized using conservative tracers, tritiated water (HTO), and chloride (^{36}Cl) with a flow rate of 20 µL min^{-1}, in our earlier studies [40] and determined to be heterogeneous. The experimental setup has been presented in Fig. 1.

Particle analysis

Particle sizes and concentrations of the solutions were analyzed with Malvern´s Zetasizer Nano ZS to determine the success of colloid separation in batch sorption experiments as well as the colloid breakthrough in the column experiment. This was done by measuring the derived count rate (DCR) and hydrodynamic particle diameter (Z-ave) values by utilizing the dynamic light scattering (DLS) technique. DCR value tells how many photons within a second arrive at the detector and thus what is the particle concentration of the solution, whereas Z-ave tells the average size of the particles. As the DCR value correlates with colloid concentration, it can be used to estimate the concentration of colloid-like particles in the samples. Nevertheless, DCR is not directly proportional to colloid concentration and is thus just an estimation.

A previously determined calibration curve for colloid concentration was used in this study [48]. To generate the calibration curve, colloid concentration was determined with two different methods: through DLS and inductively coupled plasma mass spectrometry (ICP-MS). ICP-MS (Agilent 7500ce) was used to determine the structural formula of MX-80 from the aluminum concentration in bentonite colloid dispersions, from which it was possible to back-calculate colloid concentration. With DLS, DCR was measured. By comparing measured DCR and calculated colloid concentration to each other, a calibration curve was created. As bentonite is a heterogeneous substance, there is no standard to be used to determine its concentration and thus this kind of estimation has been developed. The calibration curve was used in the preparation of diluted colloid solutions with a particle concentration of 0.1 g L^{-1} for the column experiment. For batch sorption experiments, the colloid solution with a particle concentration of 3.4 g L^{-1} was used.

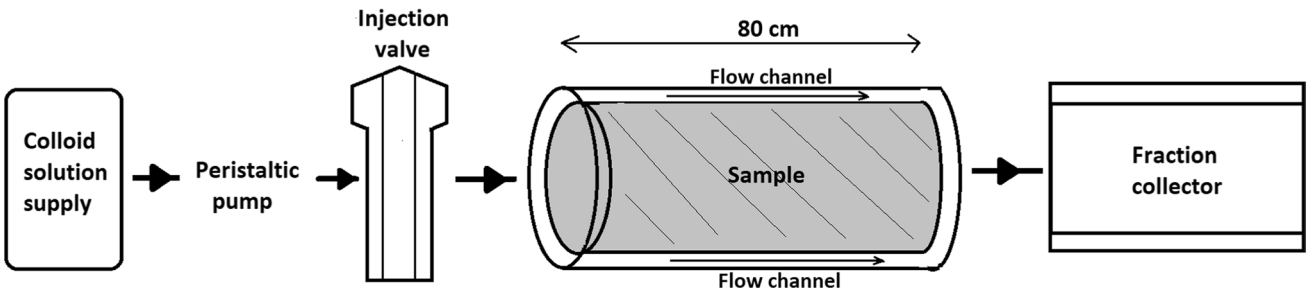

Fig. 1 The experimental setup of the column experiment. An intact 80 cm long metatexitic gneiss drill core was placed in an acrylic tube for the water phase column experiment. The experimental setup consists of a peristaltic pump, a radionuclide injection system, and a flow channel between the rock core and the plastic tube

Gamma measurements of strontium

Hidex Automatic Gamma Counter was utilized to measure the ^{85}Sr activity of the samples. The structure of the device (Hidex AGC) includes sodium iodide crystal NaI(TI) and a photomultiplier tube. The efficiency of the Hidex AGC for ^{85}Sr was about 17.2% and the detection limit MDA (minimum detectable activity) was determined to be 0.5 Bq mL^{-1} for 5.0 mL.

Molecular modeling

Quantum Mechanics optimized unit cell structures for Mg-rich phlogopite e.g., biotite [30, 31] and Mg-substituted Na-montmorillonite [49] were utilized to study the sorption of Sr(II) onto these mineral surfaces.

The calculations were performed for phlogopite systems using the CASTEP (Cambridge seral total energy package by Clark et al. [50]) code implemented into Materials Studio version 2020 [51]. The exchange correlation was described with a generalized gradient approximation GGA-PBE. As a compromise between the accuracy and computational time of calculations, the ultrasoft pseudopotentials were used for each element. The used potentials were Al_00PBE.usp for aluminum, H_00PBE.usp for hydrogen, K_00PBE.usp for potassium, Mg_00.usp for magnesium, O_soft00.usp for oxygen, Si_soft00.usp for silicon and Sr_00PBE.usp for strontium. The kinetic cut-off energy for a plane wave expansion of the wave function was 310 eV. Strontium sorption was performed only on the edge surfaces of phlogopite.

In the case of montmorillonite, all the calculations were performed with cluster models. The cluster models were generated from the earlier optimized montmorillonite structure, containing 200 mg H_2O/1 g montmorillonite. The repeat unit of the structure is shown in Fig. 2. Sorption studies were performed on basal and edge surfaces of montmorillonite. In the case of the basal surfaces, sorption onto the TOT layer ($Si_{48}Al_{19}Mg_4O_{103}(OH)_{54}$) where no cations and water molecules exist (Fig. 3a) was considered. To obtain charge neutrality in the case of strontium sorption, one or two hydroxyl groups were removed from the model structure, respectively. In the case of the edge surfaces, the sorption was supposed to happen onto the cut surface of the TOT layer, $Si_{40}Al_{14}Mg_2O_{87}(OH)_{41}$, and the charge neutrality of the model was controlled with sodium cations (6 Na^+) surrounded by water molecules (Fig. 3b).

The sorption calculations for montmorillonite systems were performed using the density functional DMol3 code implemented into BIOVIA Materials Studio 2017 R2 [52]. The atomic orbitals were specified with DNP (Double Numerical plus Polarization) including polarization functions on all atoms. The core electrons were described using DFT semi-core pseudopotentials. In the calculations, the total electronic energy and overall electronic density distribution were solved to define the energetically stable montmorillonite structures [53].

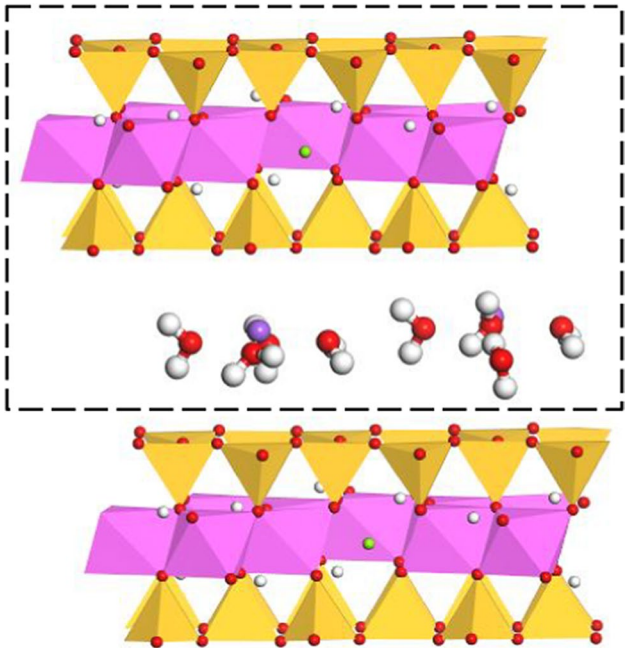

Fig. 2 The montmorillonite structure: the dashed line marked area describes the periodic model. Tetrahedral sheet: silicon—yellow. Octahedral sheet: aluminum—pink and magnesium—green. Interlayer: sodium—purple, oxygen—red, and hydrogen—white. (Color figure online)

Results and discussion

As the groundwater pH in Finland varies between pH 7 and 9 [2], these two pH conditions were chosen to be used in batch sorption experiments. Errors in experimental results can be estimated to be due to random errors and NaOH used to adjust the pH of the solutions, as Na(I) can block strontium's sorption sites. The presence and the effect of other competing bivalent ions, such as Ca(II), on strontium's sorption should also be acknowledged [54]. Differences in the results of the two pH conditions are not always easy to distinguish, and this could be explained by a small concentration of added activity (10^{-12} M) and ionic strength.

Batch sorption

Distribution coefficients K_d ($m^3\ kg^{-1}$) obtained for strontium on crushed metatexitic gneiss were not observed to vary much between the two pH conditions (Table 3). As sorption was studied as a function of time, kinetic modeling was

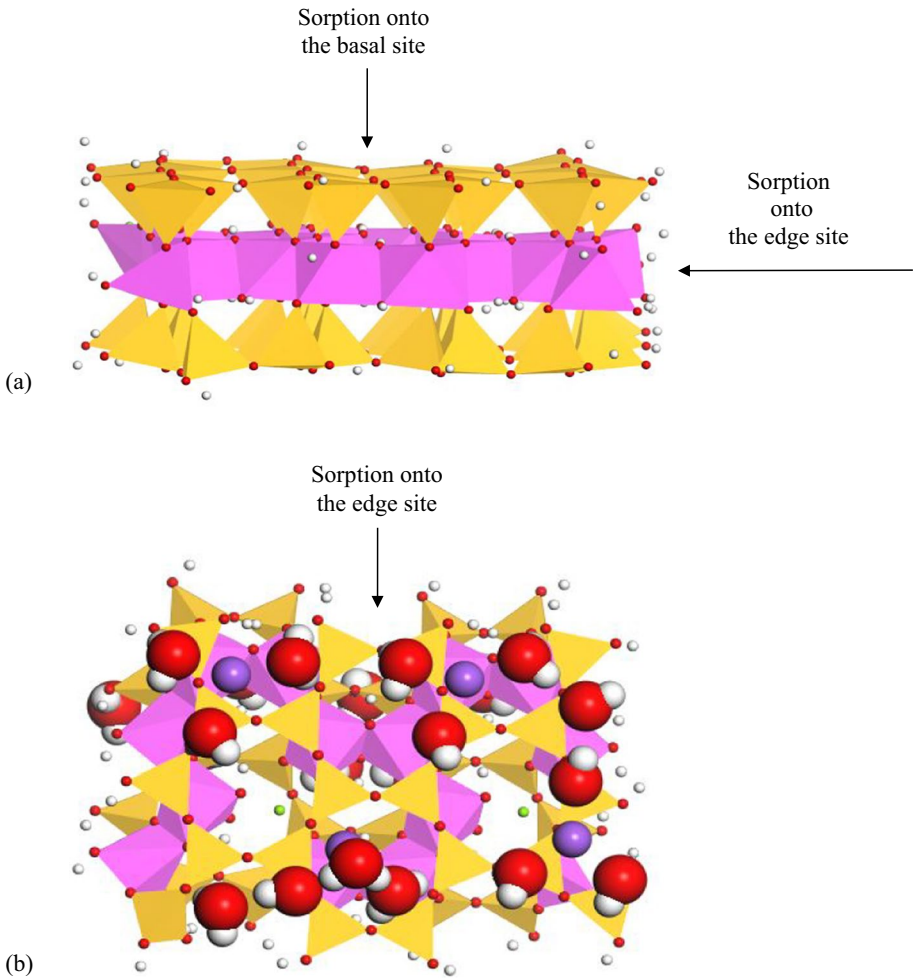

Fig. 3 The cluster models for sorption studies on the Na-montmorillonite. **a** Sorption direction onto basal and edge sites are represented. **b** The cluster model with the interlayer sodium cations and water molecules is shown. Tetrahedral sheet: silicon—yellow. Octahedral sheet: aluminum—pink and magnesium—green. Others: sodium—purple, oxygen—red, and hydrogen—white. (Color figure online)

Table 3 Distribution coefficients K_d (m^3 kg^{-1}) of Sr(II) for metatexitic gneiss

Time	K_d ($\times 10^{-3}$) (m^3 kg^{-1})	
	pH 7	pH 9
1 day	9.8 ± 0.6	10.7 ± 0.1
4 days	22.0 ± 0.8	20.5 ± 0.3
1 week	17.5 ± 0.3	19.2 ± 1.1
3 weeks	24.1 ± 3.7	23.7 ± 0.8
Average	18.3 ± 5.5	18.5 ± 4.8

used to fit the experimental findings. Like in the literature, pseudo-second-order modeling was found to describe strontium's sorption kinetics the best [55–57]. Figure 4 shows how strontium's sorption rate is rapid in the beginning, but with time the rate of sorption slows down. The result of the kinetic modeling implies that strontium´s sorption rate is limited by chemisorption. Since 1 week's results deviated from the rest of the data points, they were excluded from the kinetic modeling and have been marked in Fig. 4 with red.

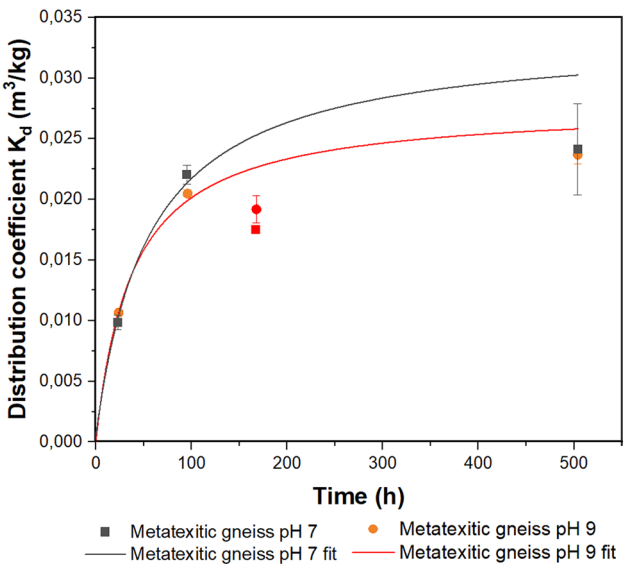

Fig. 4 Sr(II) sorption on metatexitic gneiss as a function of time and in the presence of colloids. The pseudo-second-order kinetic model showed that strontium´s sorption rate was limited by chemisorption

Table 4 Parameters for fitted pseudo-second-order kinetic model

	q_e ($\times 10^{-3}$) (m^3 kg^{-1})	k_2	R^2
pH7	33.50 ± 3.87	0.54 ± 0.19	0.99
pH9	27.75 ± 1.48	0.95 ± 0.16	0.99

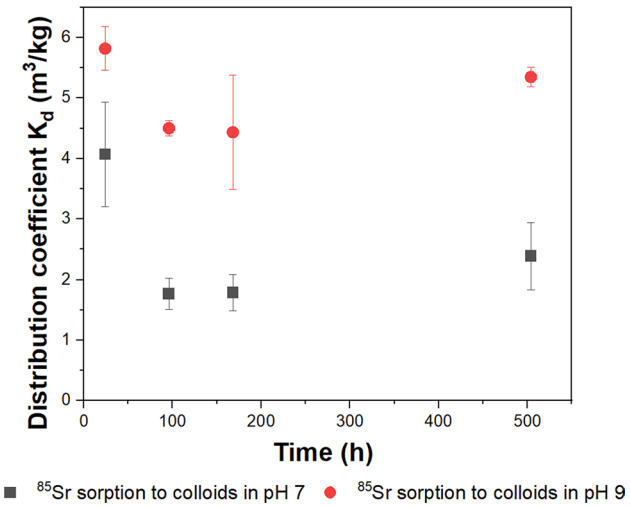

Fig. 5 Sr(II)'s sorption on colloids as a function of time and in the presence of metatexitic gneiss. Changes in sorption followed a similar trend with both used pHs, but in pH 9 strontium was more strongly sorbed on the colloid surfaces

The average K_d value at pH 7 was determined to be $(18.3 \pm 5.5) \times 10^{-3}$ m^3 kg^{-1} and at pH 9 $(18.5 \pm 4.8) \times 10^{-3}$ m^3 kg^{-1}. Previously in literature distribution coefficient values of $(84.0 \pm 1.0) \times 10^{-3}$ m^3 kg^{-1} for biotite and $(111.0 \pm 1.0) \times 10^{-3}$ m^3 kg^{-1} for metatexitic gneiss have been determined for another bivalent ion Ba(II) [21]. Through kinetic modeling, q_e-values of $(33.50 \pm 3.87) \times 10^{-3}$ m^3 kg^{-1} at pH 7 and $(27.75 \pm 1.48) \times 10^{-3}$ m^3 kg^{-1} at pH 9 were received (Table 4). Both experimental and kinetic modeling results imply that strontium's sorption on crushed metatexitic gneiss is independent of pH in this study.

Strontium's distribution coefficient values for colloids were found to be higher at pH 9 than at pH 7. Whereas strontium's sorption on metatexitic gneiss followed pseudo-second-order kinetics, strontium's sorption on colloids in the presence of metatexitic gneiss was governed by desorption as a function of time. In Fig. 5 it can be seen how strontium sorbed on colloids desorbs due to the competition between metatexitic gneiss rock surface and colloid surfaces. As the used experimental setup did not allow us to confirm if all the Sr(II) sorbed on the surface of metatexitic gneiss originated from the colloid surfaces and not, for example, from loose strontium ions in the solution, kinetic modeling was not applied to colloid results. Nevertheless, it is still

Table 5 Distribution coefficients K_d (m^3 kg^{-1}) of Sr(II) for colloids

Time	K_d (m^3 kg^{-1})	
	pH 7	pH 9
1 day	4.1 ± 0.9	5.8 ± 0.4
4 days	1.8 ± 0.3	4.5 ± 0.1
1 week	1.8 ± 0.3	4.4 ± 0.9
3 weeks	2.4 ± 0.6	5.4 ± 0.2
Average	2.5 ± 0.9	5.0 ± 0.6

Table 6 Sorption and desorption percentages of metatexitic gneiss experiments. The presented results are an average of two parallel samples

Time	Sorption (%)		Desorption (%)	
	pH 7	pH 9	pH 7	pH 9
1 day	52.1 ± 1.1	54.3 ± 0.2	14.5 ± 1.5	12.5 ± 0.5
4 days	70.3 ± 0.2	69.4 ± 0.2	10.2 ± 0.1	9.3 ± 0.3
1 week	65.9 ± 0.4	68.1 ± 0.9	11.8 ± 0.8	8.3 ± 0.4
3 weeks	72.6 ± 2.2	72.5 ± 0.5	6.1 ± 0.9	6.0 ± 0.5
Average	65.2 ± 8.0	66.1 ± 7.0	10.7 ± 3.1	9.0 ± 2.3

observable that at pH 9 fewer strontium ions shift from the colloid solution phase to the metatexitic gneiss surface than at pH 7, implying that strontium is more strongly attached on the colloid surface in higher pHs. The average K_d value for colloids at pH 7 was determined to be 2.5 ± 0.9 m^3 kg^{-1} and for pH 9 5.0 ± 0.6 m^3 kg^{-1} (Table 5).

Throughout the experiment, the sorption percentage of metatexitic gneiss was found to range between 50 and 70% whereas the desorption percentage ranged between 6 and 15% (Table 6). Results show that strontium's overall sorption strength to rock's minerals in the presence of colloids is not very strong [58] and thus only a mediocre amount of retention is expected to happen. Based on the low desorption percentage values received, sorbed strontium does not seem to desorb very eagerly from the metatexitic gneiss surface once attached. Resuspension to the liquid phase is slightly greater at pH 7 at every time point, but otherwise, the effect of pH on strontium's sorption/desorption on metatexitic gneiss was not observed (Fig. 6).

With colloids, strontium's overall sorption percentage in the presence of metatexitic gneiss was approximately 95% at its highest, and sorption remained strongest at pH 9 in every experimental setup (Table 7). When colloids were rinsed with fresh groundwater simulant, 6–19% of the suspended radionuclides resuspend from the colloid surfaces. In this case, the differences between the two pHs are not distinct, which could imply that the more loosely attached or free strontium ions had already shifted from the colloid solution to the surface of the crushed metatexitic gneiss during the initial sorption experiment and that low-saline groundwater

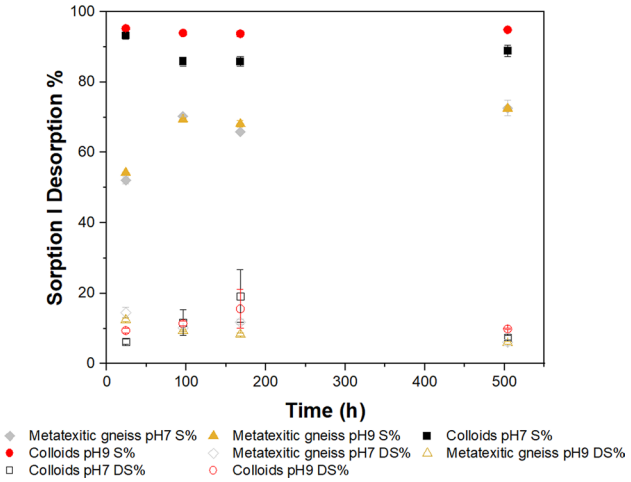

Fig. 6 Sorption and desorption percentages of Sr(II) for metatexitic gneiss and colloids

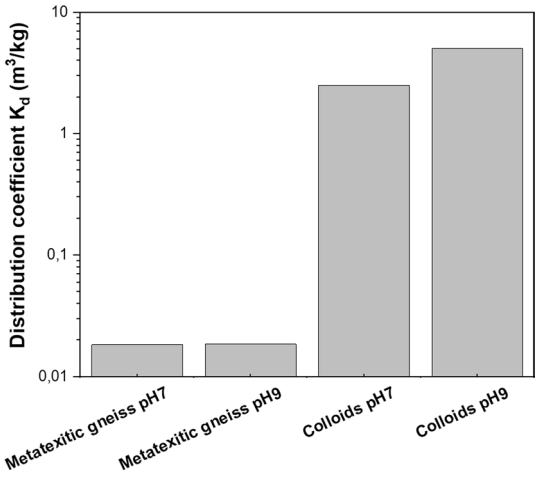

Fig. 7 Strontium´s sorption on metatexitic gneiss and colloids. Received K_d values for colloids were found to be 100 times greater than the ones for metatexitic gneiss

Table 7 Sorption and desorption percentages of colloid experiments

Time	Sorption (%)		Desorption (%)	
	pH 7	pH 9	pH 7	pH 9
1 day	93.2 ± 1.0	95.2 ± 0.2	6.3 ± 0.7	9.4 ± 0.7
4 days	85.8 ± 1.3	93.9 ± 0.1	11.7 ± 3.7	11.4 ± 0.7
1 week	85.9 ± 1.4	93.7 ± 0.9	19.2 ± 7.5	15.6 ± 5.6
3 weeks	88.9 ± 1.6	94.8 ± 0.1	7.4 ± 0.7	9.9 ± 0.2
Average	88.4 ± 3.0	94.4 ± 0.6	11.2 ± 5.1	11.6 ± 2.4

The presented results are an average of two parallel samples

simulant is not strong enough to break the bonds between the radionuclide and the colloid surface.

Batch sorption experiments showed that strontium's sorption on metatexitic gneiss did not seem to be dependent on pH. This could have been due to the low strontium concentration (10^{-12} M) in the samples, which prevented surface complexation with carbonate from taking place at pH 9 [46]. Desorption´s pH dependency was not distinct either.

When sorption percentages concerning the colloids were inspected, dependency on pH was detected. As colloids are known to have a higher negative charge at pH 9, this result was expected [59]. In comparison with distribution coefficient values obtained on crushed metatexitic gneiss, values on colloids remained a hundred times greater on average even though some of the strontium desorbed from the colloid surface due to the sorption competition (Fig. 7). When colloids were later rinsed with groundwater simulant, there was no observable pH dependency.

Sorption results were also affected by the notable difference between the specific surface areas of metatexitic gneiss and colloids. As montmorillonite particles have a larger specific surface area per unit volume than crushed rock, a greater number of binding sites enables colloids to bind more radionuclides. Unfortunately, the specific surface area for montmorillonite colloids could not be determined in this experiment, and thus the comparison of specific surface areas can only be done between metatexitic gneiss (SSA = 0.5–1.0 m^2 g^{-1} ± 5% [21]) and montmorillonite clay particle (SSA = 760.0–810.0 m^2 g^{-1} [43]).

It is known, that for colloids to be relevant in radionuclide transport, the radionuclide's affinity to the colloid surface needs to be significantly stronger than to the rock surface [29]. Additionally, in longer time scales desorption from colloids' surface should not be substantial. Concerning this study, strontium's affinity to colloid surfaces is much stronger than it is to rock surfaces, but it is debatable if desorption from colloid surfaces is too significant and fast for colloids to have a considerable role in transporting strontium outside of the repository system after canister failure.

Molecular modeling

Molecular modeling was performed in parallel with the experimental work to assess the sorption affinity at the molecular level. Sorption of Sr(II) was calculated and studied onto biotite end-member mineral phlogopite (model mineral for metatexitic gneiss) and Na-montmorillonite (model mineral for bentonite) surfaces. In the case of phlogopite, two edge sites were considered: a cut surface and a frayed edge site (Fig. 8). In the case of montmorillonite, sorption studies were performed for a basal site and an edge site (Fig. 9).

The sorption energies are listed in Table 8. The Sr(II) sorption energies on the montmorillonite surface are twice as strong as on the phlogopite surfaces, indicating higher

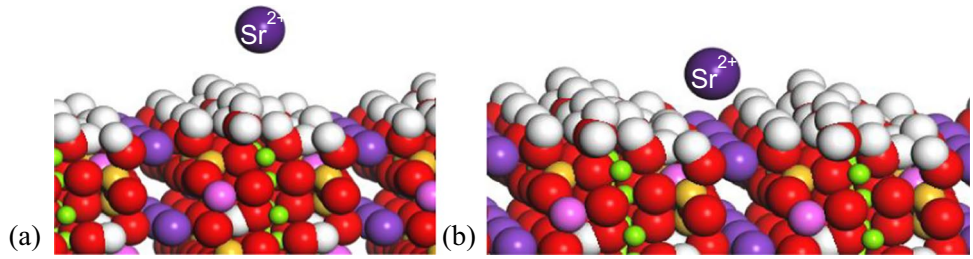

Fig. 8 The optimized sorption positions of Sr(II) on two edge sites of phlogopite: **a** a cut surface and **b** a frayed edge site. Aluminum—pink. Hydrogen—white. Magnesium—green. Oxygen—red. Silicon—yellow. Sodium—purple. (Color figure online)

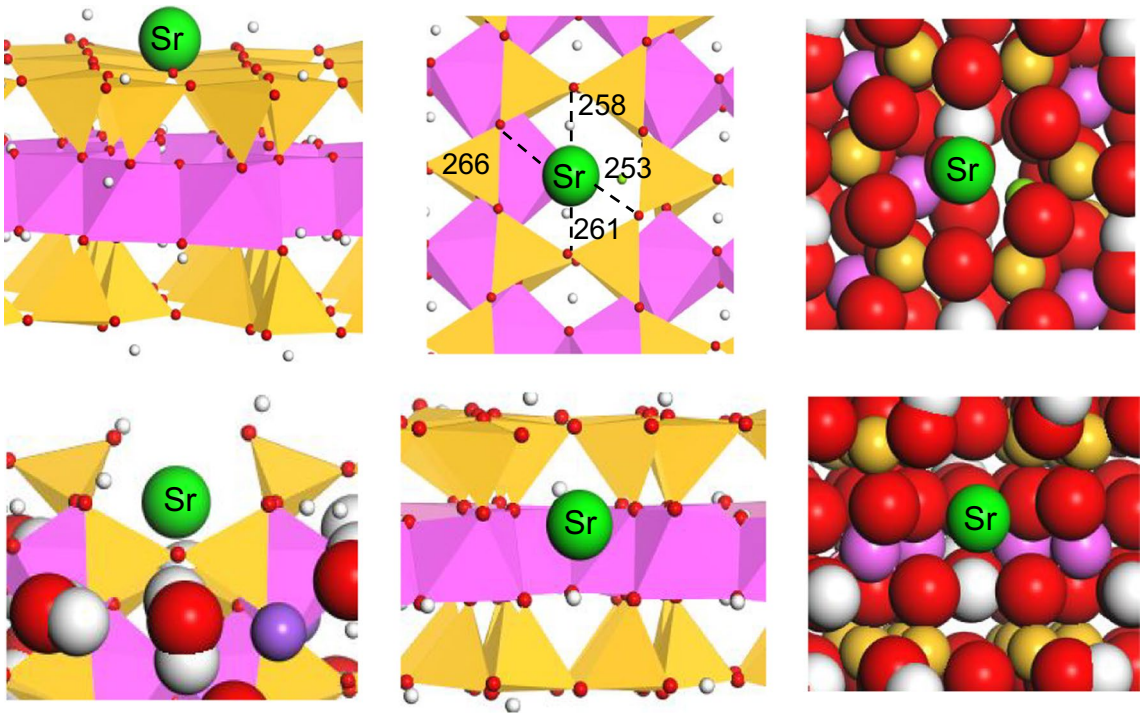

Fig. 9 Sorption positions of Sr(II) ion onto the TOT layer and edge site of the montmorillonite. A side view on the left, a top view in the middle, and a top view with van der Waals spheres on the right. Tetrahedral sheet: silicon—yellow. Octahedral sheet: aluminum—pink. Others: sodium—purple, oxygen—red, hydrogen—white, and strontium—green. (Color figure online)

mobility of strontium in solution where bentonite colloids exist. Sr(II) is a moderately sorbing radionuclide and it favors the sorption on bentonite instead of metatexitic gneiss. Results of molecular modeling complement well and ascertain results gained experimentally by batch sorption experiments where strontium sorption on bentonite was a hundred times greater than on metatexitic gneiss.

Column experiment

Colloid breakthrough from the metatexitic gneiss column was studied by measuring the particle concentration of every 50th sample. Colloid solutions used in column experiments had DCR values of 900–1200 kcps, which corresponds to about 0.15 g L^{-1} of colloids in the solution. Colloid breakthrough from the rock column varied greatly and on average 40% of the total colloid volume was able to break through during 44 days. The colloids used in this experiment had relatively large sizes (300–500 nm) which may have influenced the interaction between the colloids and the artificial fracture

Table 8 Sorption energies of Sr(II) onto phlogopite and Na-montmorillonite surfaces

Mineral	Sorption site	Ion	Charge of the model	Sorption energy (eV)
Phlogopite	Edge site	Sr(II)	+2	−7.54
	Frayed edge site	Sr(II)	+2	−7.95
Montmorillonite	Basal site	Sr(II)	0	−14.79
		Sr(II)	−1	−17.86
	Edge site	Sr(II)	0	−16.20

surface and thus increased the colloid mobility [29]. Besides colloid size, the colloid breakthrough was also affected by whether the colloids were filtered within rock pores, column tubes, or retained within stagnant pools of flow channels.

Metatexitic gneiss´s pore structure and porosity have been studied earlier in the REPRO project [36, 60]. The micro fissures and pores of more than 1 µm are rare in this rock type and the porosity is more pronounced in biotite and altered cordierites consisting of intragranular nanometer-scale pores. When colloids retain from the flow within the pores of the rock, the system stabilizes, and more colloids can go through. The water flow rate used was the fastest possible (50 µL min^{-1}) in these experimental conditions, diminishing the effect of sedimentation caused by gravitational forces and preventing colloids from suspending on rock surfaces.

Strontium's breakthrough in the metatexitic gneiss column was found successful. The initial activity of 10.18 kBq was injected into the column system as a pulse and the highest peak of activity was reached quite early, already between hours 50 and 65, reaching as high as 2.96 Bq mL^{-1}. After this, the activity breakthrough decreased slowly until it reached the background level. Approximately 3.90 L of colloid solution was pumped into the system. A total amount of 4.35 kBq came through the column, giving a recovery of 42.7% with a collection time of roughly 1800 h. Compared to earlier studies with the same column, recoveries of 98% and 97% were received for the conservative tracers HTO and Cl-36, respectively, with a 5300 h collection time [40].

Non-conservative strontium's breakthrough with colloids from the column was observed to be faster than the conservative tracers' [40]. This phenomenon, a hydrodynamic chromatography effect, has been recognized earlier in the literature [29, 61, 62]. Instead of being slowed down by migrating through the whole flow profile, the tracer is transported with the colloid in the middle of the fracture. The result shown in Fig. 10 has been decay corrected and the level of the background has been marked with a straight red line.

The column experiment was terminated after 3 months' experimental time, which was limited by the tracer's short half-life (64.84 days). When background levels were reached, 60% of the injected activity was still retained within the system. Strontium's high mobility can be observed from the results of the column experiment: The breakthrough was greatest at the beginning of the experiment, followed by a slowly decreasing slope of activity until the background level and the detection limit of the radiometric measurement were reached, and the experiment was terminated. In the beginning, tracers that have not sorbed to the metatexitic gneiss surface will be transported with colloids and as free radionuclides from the column via groundwater simulant. After this high activity peak, strontium nuclides that were first retained on the rock surface start to desorb and resuspend to the liquid phase. Migration out of the column decreases with time as the permeability of the column decreases through colloid filtration and clogging. The shape of strontium´s breakthrough curve was found to correspond well with the one determined earlier by Voutilainen et al. [19] with the same column.

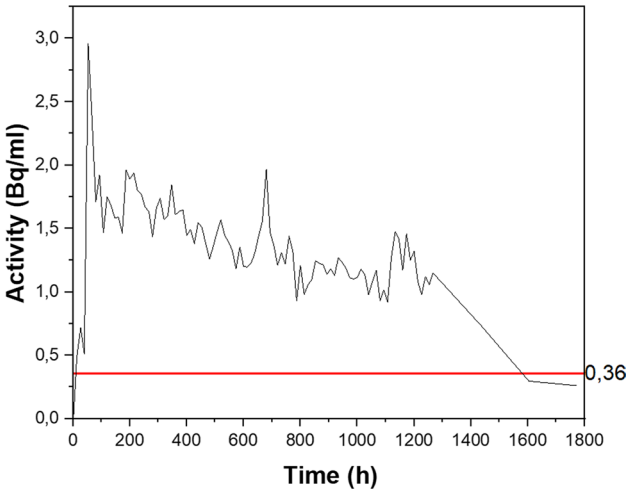

Fig. 10 Sr(II)'s breakthrough from the metatexitic gneiss column. Sr(II)'s breakthrough activity concentration (Bq mL^{-1}) has been presented as a function of time in the metatexitic gneiss column experiment with a flow rate of 50 µL min^{-1}. The largest activity peak was reached at an early stage, just a few days after the start of the experiment

Column experiment results are consistent with batch sorption experiments. They are also consistent with molecular modeling results, which indicate that strontium can sorb rather strongly onto rock surfaces, but even more so on colloids. Had the strontium's affinity on the rock surface been stronger or more on par than it was on the colloid surface, strontium's breakthrough may not have been observed in the same magnitude as it was, or it could have been much slower [29]. As the largest breakthrough of strontium was detected in an early phase of the experiment, the presence of free or colloidal strontium in groundwater could be speculated to be high at the early stages of possible SNF leakage.

Bentonite water is expected to increase the pH of groundwater in the near vicinity of bentonite buffer, but as the natural pH of groundwater at the repository level varies between 7.3 and 8.8 [2] pH 7 colloid solution was chosen to be used in column experiments. In higher pH conditions, colloids are more stable than they are in neutral media and this stability is seen in colloid-facilitated transport with less aggregation and sedimentation [15]. It could be speculated, that if pH 9 colloid solution was used in the column experiment, strontium's sorption towards colloids could have further increased due to a more negative colloid surface charge and more strontium could have broken through the column.

As the current saline Finnish groundwater conditions do not seem to favor colloid formation, stability, or sorption towards colloids, colloid-facilitated radionuclide transportation is ultimately inhibited. However, the salinity and the pH of groundwater are expected to change due to the possible intrusion of post-glacial melting waters or land uplift. As strontium has a relatively short half-life, the activities of strontium isotopes in SNF have been halved several times and most likely ceased to exist by the time the changes in the groundwater condition are expected to happen [63]. This emphasizes the role of colloids in the migration of longer-lived radionuclides such as actinides. Even though strontium´s colloid-facilitated transport is not directly applicable in the current state of the Finnish repository system and its prevailing environmental conditions, in the countries where the groundwater is less saline the study of strontium´s migration stays relevant to this present day as well. This is the case, for example, in Grimsel, Switzerland [2].

These experiments were done in simplified laboratory conditions at normal room temperature and thus will not represent real environmental conditions. In the future, the flow rate's effect on sorption and migration could be studied by repeating the column experiment with a slower flow rate. Further, more complex systems should be studied and the effect of higher temperatures on the properties and structure of bentonite buffer and colloids should be addressed.

Conclusions

Strontium's sorption on biotite-rich metatexitic gneiss and MX-80 bentonite colloids was studied with batch sorption and desorption experiments. In addition, colloids' effect on strontium's migration in flow within the granitic drill core column was determined. Molecular modeling techniques were used to assess strontium's sorption affinity and the probability of certain sorption sites, as well as to justify the experimental findings. Furthermore, particle analysis was utilized to characterize colloids in the solutions.

The distribution coefficient value of $(1.8 \pm 0.6) \times 10^{-2}$ m^3 kg^{-1} was determined at pH 7 and $(1.9 \pm 0.5) \times 10^{-2}$ m^3 kg^{-1} at pH 9 for crushed metatexitic gneiss. For montmorillonite (colloids), a distribution coefficient value of (2.5 ± 0.9) m^3 kg^{-1} was determined at pH 7 and (5.0 ± 0.6) m^3 kg^{-1} at pH 9 through batch sorption experiments. Distribution coefficient values determined for montmorillonite were found to be approximately a hundred times greater than the ones determined for metatexitic gneiss. Strontium's affinity for colloids in the presence of metatexitic gneiss was more dependent on pH. On average, desorption from montmorillonite was slightly greater, but there was no significantly observable pH dependency for either metatexitic gneiss´s or colloids´ desorption when rinsed with groundwater simulant. Kinetic modeling was used to fit experimentally received K_d values for metatexitic gneiss. Strontium´s sorption kinetics were found to follow a pseudo-second-order model, where sorption is limited by chemisorption. Equilibrium capacity values of $(33.50 \pm 3.87) \times 10^{-3}$ m^3 kg^{-1} at pH 7 and $(27.75 \pm 1.48) \times 10^{-3}$ m^3 kg^{-1} at pH 9 for strontium´s sorption on metatexitic gneiss were received.

Strontium´s sorption sites in metatexitic gneiss biotite (phlogopite) were determined to be on the edge and frayed edge sites whereas sorption to montmorillonite was found to take place on the basal plane and edge site. With molecular modeling, the sorption energies of Sr(II) on the metatexitic gneiss's phlogopite were determined to be − 7.54 eV on the edge site and − 7.95 eV on the frayed edge site. For montmorillonite, sorption energies were determined to be − 14.79 eV and − 17.86 eV on the basal site and − 16.20 eV on the edge site. The sorption energies of Sr(II) on the montmorillonite surface were determined to be twice as strong as on the phlogopite surfaces, implying that Sr(II) is a mobile radionuclide as it favors the sorption onto bentonite colloids instead of biotite in the granitic rock.

Strontium´s breakthrough from the granitic drill core column was successful. The breakthrough was not only influenced by radionuclide properties but also by colloid breakthrough. The recovery of 42.7% for strontium (free or colloidal) and 40% for pure colloids was obtained. Thus, the results imply that most of the strontium that broke through the column migrated with colloids, and had the experiment been continued further, more strontium may have been recovered. The presence of colloids was found to fasten the breakthrough time of strontium in comparison with the breakthrough results determined for conservative tracers in our earlier experiments.

The results of this study suggest that bentonite colloids originating from the bentonite buffer can act as transporters of strontium in a fracture system.

Acknowledgements The authors wish to acknowledge CSC—IT Center for Science, Finland, for computational resources. The project leading to this application has received funding from the European Union's Horizon 2020 research and innovation program under grant agreement No 847593. Funding has also been received from the Fortum and Neste Foundation under grant agreements No 20210117 and 20220097.

Funding Open Access funding provided by University of Helsinki including Helsinki University Central Hospital.

Declarations

Conflict of interest The authors declare no conflict of interest.

References

1. Geier J, Bath A, Stephansson O (2012) Comparison of site descriptive models for Olkiluoto, Finland and Forsmark. STUK-TR, Sweden, p 14
2. Hellä P, Pitkänen P, Löfman J, Partamies S, Vuorinen U, Wersin P (2014) Safety case for the disposal of spent nuclear fuel at Olkiluoto: definition of reference and bounding groundwaters, buffer and backfill porewaters. Posiva report 2014-04, Posiva
3. POSIVA (2012) Safety case for the disposal of spent nuclear fuel at Olkiluoto: Description of the disposal system. Posiva report 2012-05
4. POSIVA (2017) Safety case plan for the operating license application. Posiva report 2017-02, p 151
5. Poteri A, Nordman H, Pulkkanen V-M, Smith P (2014) Radionuclide transport in the repository near-field and far-field. Posiva report 2014-02, Posiva
6. Karvonen TH, Sacklén N (2020) Material of the disposal facility: update of estimated quantities. Posiva working report 2020-03, Posiva
7. Chegbeleh LP, Nishigaki M, Akudago JA, Alim MdA, Komatsu M (2008) Concepts of repository and the functions of bentonite in repository environments: a state of the art review. J Fac Env Sci Tech 13:1–5
8. IAEA (2005) Statements of the deputy directors general, international conference on the safety of radioactive waste disposal. http://www.iaea.org/NewsCenter/Statements/DDGs/2005/taniguchi03102005.html, Accessed 14 Dec 2022
9. Sellini P, Leupin OX (2013) The use of clay as an engineered barrier in radioactive waste management: a review. Clays Clay Miner 61:477–498
10. Meunier A, Velde B (2008) The origin of clay minerals in soils and weathered rocks. Springer, Berlin
11. Missana T, Alonso U, Fernandez AM, Garcia-Gutierrez M (2018) Colloidal properties of different smectite clays: significance for the bentonite barrier erosion and radionuclide transport in radioactive waste repositories. Appl Geochem 97:157–166
12. Eggloffstein T (2001) Natural bentonites: influence of the ion exchange and partial desiccation on permeability and self-healing capacity of bentonites in GCLs. Geotext Geomembr 19:427–444
13. Aiken GR, Hsu-Kim K, Ryan JN (2011) Influence of dissolved organic matter on the environmental fate of metals, nanoparticles and colloids. Environ Sci Technol 45:3196–3201
14. Uddin F (2008) Clays, nanoclays, and montmorillonite minerals. Metall Mater Trans A 39:2804–2814
15. García-García S, Jonsson M, Wold S (2006) Temperature effect on the stability of bentonite colloids in water. J Colloid Interface Sci 298:694–705
16. Neretnieks I (1980) Diffusion in the rock matrix: an important factor in radionuclide retardation? J Geophys Res 85:4379–4397
17. Poteri A, Nordman H, Pulkkanen V.M, Hautojärvi A, Kekäläinen P (2012) Representing solute transport through the multi-barrier disposal system by simplified concepts. Posiva report 2012-20, Posiva
18. Soler JM, Landa J, Havlova V, Tachi Y, Ebina T, Sardini P, Siitari-Kauppi M, Eikenberg J, Martin AJ (2015) Comparative modeling of an in situ diffusion experiment in granite at the Grimsel Test Site. J Cont Hydrol 179:89–101
19. Voutilainen M, Kekäläinen P, Poteri A, Siitari-Kauppi M, Helariutta K, Andersson P, Nilsson K, Byegård J, Skålberg M, Yli-Kaila M, Koskinen L (2019) Comparison of water phase diffusion experiments in laboratory and in situ conditions. J Hydrol 575:716–729
20. Muuri E, Ikonen J, Matara-aho M, Lindberg A, Holgersson S, Voutilainen M, Siitari-Kauppi M, Martin A (2016) Behavior of Cs in Grimsel granodiorite: sorption on main minerals and crushed rock. Radiochim Acta 104:575–582
21. Muuri E, Matara-aho M, Puhakka E, Ikonen J, Martin A, Koskinen L, Siitari-Kauppi M (2018) The sorption and diffusion of Ba-133 in crushed and intact granitic rocks from the Olkiluoto and Grimsel in-situ test sites. Appl Geochem 89:138–149
22. Kyllönen J, Hakanen M, Lindberg A, Harjula R, Vehkamäki M, Lehto J (2014) Modeling of cesium sorption on biotite using exchange selectivity coefficients. Radiochim Acta 102:919–929
23. Kersting AB, Efurd DW, Finnegan DL, Rokop DJ, Smith DK, Thompson JL (1999) Migration of plutonium in ground water at the Nevada test site. Nature 397:56–59
24. Novikov AP, Kalmykov SN, Utsunomiya S, Ewing RC, Horreard F, Merkulov A, Clark SB, Tkachev VV, Myasoedov BF (2006) Colloid transport of plutonium in the far-field of the Mayak production association, Russia. J Sci 314:638–641
25. Puls RW, Powell RM (1992) Transport of inorganic colloids through natural aquifer material: Implications for contaminant transport. Environ Sci Technol 26:614–621
26. Vilks P, Baik M (2001) Laboratory migration experiments with radionuclides and natural colloids in a granite fracture. J Contam Hydrol 47:197
27. Takala M, Manninen P (2008) Sampling and characterisation of groundwater colloids in ONKALO at Olkiluoto, Finland in 2007. Posiva working report 2008-32, Posiva
28. Vuorinen U, Hirvonen H (2005) Bentonite as a colloid source in groundwaters at Olkiluoto. Posiva working report 2005-3, Posiva
29. Wold S (2010) Sorption of prioritized elements on montmorillonite colloids and their potential to transport radionuclides. Technical Report TR-10-20, SKB
30. Puhakka E, Olin M (2014) In: Rabung T, García D, Montoya V, Molinero J, (eds) Final workshop proceedings of the collaborative project "Crystalline ROCK retention processes" (7th EC FP CP CROCK), KIT scientific report 7656. KIT Scientific Publishing, Karlsruhe
31. Puhakka E, Li X, Ikonen J, Siitari-Kauppi M (2019) Sorption of selenium species onto phlogopite and calcite surfaces: DFT studies. J Contam Hydrol 227:103553
32. Viani A, Gualtieri AF, Artioli G (2002) The nature of disorder in montmorillonite by simulation of X-ray powder patterns. Am Min 87:966–975
33. ASTM (American Society of Testing Materials) (1984) Standard test method for distribution ratios by the short-term batch method. Ann Book ASTM Stand D 4319–83:619–624
34. Ho YS, McKay G (1999) Pseudo-second order model for sorption processes. Process Biochem 34:451–465
35. Kärki A, Paulamäki S (2006) Petrology of Olkiluoto. Posiva Report 2006-02
36. Sammaljärvi J, Lindberg A, Voutilainen M, Kuva J, Ikonen J, Johanson B, Siitari-Kauppi M, Pitkänen P, Koskinen L (2017) Multi-scale study of the mineral porosity of veined gneiss and pegmatitic granite from Olkiluoto, Western Finland. J Radioanal Nucl Chem 314:1557–1575

37. Kuva J, Voutilainen M, Kekäläinen P, Siitari-Kauppi M, Sammaljärvi J, Timonen J, Koskinen L (2016) Gas phase measurements of matrix diffusion in rock samples from Olkiluoto bedrock, Finland. Transp Porous Med 115:1–20
38. Voutilainen M, Poteri A, Helariutta K, Siitari-Kauppi M, Nilsson K, Andersson P, Byegård J, Skålberg M, Kekäläinen P, Timonen J, Lindberg A, Pitkänen P, Kemppainen K, Liimatainen J, Hautojärvi A, Koskinen L (2014) In-situ experiments for investigating the retention properties of rock matrix in ONKALO, Olkiluoto, Finland. In: Annual waste management symposium (VM 2014) 3, pp 1969–1981
39. Poteri A, Andersson K, Nilsson P, Byegård J, Skålberg M, Siitari-Kauppi M, Helariutta K, Voutilainen M, Kekäläinen P, Ikonen J, Sammaljärvi J, Lindberg A, Timonen J, Kuva J, Koskinen L (2018) The first matrix diffusion experiment in the water phase of the REPRO project: WPDE 1. Posiva working report 2017-23, Posiva
40. Voutilainen M, Kekäläinen P, Kuva J, Siitari-Kauppi M, Yli-Kaila M, Koskinen L (2017) Laboratory scale advection-matrix diffusion experiment in Olkiluoto veined gneiss using H-3 and Cl-36 as tracers. MRS Adv 2:655–660
41. Kumpulainen S, Kiviranta L (2010) Mineralogical and chemical characterization of various bentonite and smectite-rich clay minerals. Posiva working report 2010-52, Posiva
42. Vuorinen U, Snellman M (1998) Finnish reference waters for solubility, sorption and diffusion studies. Posiva working report 98-61, Posiva
43. Kobayashi I, Owada H, Ishii T, Iizuka A (2017) Evaluation of specific surface area of bentonite-engineered barriers for Kozeny–Carman law. Soils Found 57:683–697
44. Allard B, Beall J (1979) Sorption of americium on geologic media. J Environ Sci Health A 14:507–518
45. Lehto J, Hou X (2011) Chemistry and analysis of radionuclides: laboratory techniques and methodology. In: Radiochemistry of the Alkali Earth Metals. Wiley-VCH, Weinheim
46. Carroll SA, Roberts SK, Criscenti LJ, O'Day PA (2008) Surface complexation model for strontium sorption to amorphous silica and goethite. Geochem Trans. https://doi.org/10.1186/1467-4866-9-2
47. Missana T, Garcia-Gutiérrez M (2007) Adsorption of bivalent ions (Ca(II), Sr(II) and Co(II)) onto FEBEX bentonite. Phys Chem Earth 32:559–567
48. Elo O, Hölttä P, Kekäläinen P, Voutilainen M, Huittinen N (2019) Neptunium(V) transport in granitic rock: a laboratory scale study on the influence of bentonite colloids. App Geochem 103:31–39
49. Seppälä A, Puhakka E, Olin M (2016) Effect of layer charge on the crystalline swelling of Na^+, K^+ and Ca^{2+} montmorillonites: DFT and molecular dynamics studies. Clay Miner 51:197–211
50. Clark S, Segall M, Pickard C, Hasnip P, Probert M, Refson K, Payne M (2005) First principles methods using CASTEP. Z Kristallogr 220:567–570
51. Dassault Systèmes (2019) BIOVIA materials studio 2020. Dassault Systèmes, San Diego
52. Dassault Systèmes (2016) BIOVIA materials studio 2017 R2. Dassault Systèmes, San Diego
53. Leach AR (2001) Molecular modelling: principles and applications, 2nd edn. Pearson Education Limited, Essex
54. Handley-Sidhu S, Mullan T, Grail Q, Albadarneh M, Ohnuki T, Macaskie LE (2016) Influence of pH, competing ions and salinity on the sorption of strontium and cobalt onto biogenic hydroxyapatite. Sci Rep. https://doi.org/10.1038/srep23361
55. Marinović S, Ajduković M, Jović-Jovičić N, Mudrinić T, Nedić-Vasiljević B, Banković P, Milutinović-Nikolić A (2017) Adsorption of strontium on different sodium enriched bentonites. J Serb Chem Soc 82:1–16
56. Abu-Nada A, Abdala A, McKay G (2021) Isotherm and kinetic modeling of strontium adsorption on graphene oxide. Nanomaterials 11:2780
57. Lee MG, Kam SK, Lee CH (2021) Kinetic and isothermal adsorption properties of strontium and Cesium ions by Zeolitic materials synthesized from Jeju volcanic rocks. Environ Eng Res 26(2):200127
58. Brookshaw DR, Pattrick RAD, Lloyd JR, Vaughan DJ (2012) Microbial effects on mineral-radionuclide interactions and radionuclide solid-phase capture processes. Mineral Mag 76:777–806
59. Večeř M, Pospisil J (2012) Stability and rheology of aqueous suspensions. Proc Eng 42:720–1725
60. Sammaljärvi J, Lindberg A, Ikonen J, Voutilainen M, Siitari-Kauppi M, Koskinen L (2014) Investigation of mineralogy, porosity and pore structure of Olkiluoto bedrock. MRS Online Proc Libr 1665:31–37
61. Geckeis H, Schäfer T, Hauser W, Rabung T, Missana T, Degueldre C, Möri A, Eikenberg J, Fierz Th, Alexander RW (2004) Results of the colloid and radionuclides retention experiment (CRR) at the Grimsel Test Site (GTS). Switzerland: impact of reaction kinetics and speciation on radionuclide speciation. Radiochim Acta 94:627–636
62. Kurosawa S, James CJ, You M, Ibaraki M (2006) Model analysis of the colloid and the radionuclide retardation experiment at the Grimsel Test Site. J Colloid Interface Sci 298:467–475
63. Read D, Black S, Buckby T, Hellmuth KH, Marcos N, Siitari-Kauppi M (2008) Secondary uranium mineralization in southern Finland and its relationship to recent glacial events. Glob Planet Change 60:235–249